Structural Stability and Phase Transitions in WO_3 Thin Films

C. V. Ramana,*,† S. Utsunomiya,† R. C. Ewing,†,‡ C. M. Julien,§ and U. Becker†

Nanoscience and Surface Chemistry Laboratory, Department of Geological Sciences, University of Michigan, Ann Arbor, Michigan 48109, Materials Science and Engineering, University of Michigan, Ann Arbor, Michigan 48109, and Institut des Nano-Sciences de Paris (INSP), CNRS-UMR 7588, Université Pierre et Marie Curie, Campus Boucicaut, 140 rue de Lourmel, 75015 Paris, France

Received: November 17, 2005; In Final Form: April 3, 2006

Tungsten oxide (WO_3) thin films have been produced by KrF excimer laser ($\lambda = 248$ nm) ablation of bulk ceramic WO_3 targets. The crystal structure, surface morphology, chemical composition, and structural stability of the WO_3 thin films have been studied in detail. Characterization of freshly grown WO_3 thin films has been performed using X-ray diffraction (XRD), atomic force microscopy (AFM), energy-dispersive X-ray spectroscopy (EDX), Raman spectroscopy (RS), transmission electron microscopy (TEM), and selected area electron diffraction (SAED) measurements. The results indicate that the freshly grown WO_3 thin films are nearly stoichiometric and well crystallized as monoclinic WO_3. The surface morphology of the resulting WO_3 thin film has grains of ~60 nm in size with a root-mean-square (rms) surface roughness of 10 nm. The phase transformations in the WO_3 thin films were investigated by annealing in the TEM column at 30−500 °C. The phase transitions in the WO_3 thin films occur in sequence as the temperature is increased: monoclinic → orthorhombic → hexagonal. Distortion and tilting of the WO_6 octahedra occurs with the phase transitions and significantly affects the electronic properties and, hence, the electrochemical device applications of WO_3.

I. Introduction

Tungsten oxide (WO_3) is an intensively studied representative of a group of "chromogenic" materials because of the coloration effects associated with various processes.[1−6] There has been a great deal of recent interest in WO_3 thin films for a wide variety of applications in optoelectronics, microelectronics, selective catalysis, and environmental engineering.[1−11] WO_3 has been in use for the development of smart windows for energy-efficient architecture of buildings and automobiles, flat-panel displays, optical memory and writing−reading−erasing devices, and electronic information displays.[1,4−6,8] It has been demonstrated that WO_3 films exhibit chemical sensing properties,[2,3,9,11] which will have numerous applications in environmental pollution monitoring. WO_3 thin films show excellent functional activity to various gases, such as H_2S, NO_x, trimethylamine, and other organic compound gases.[3] The ability to detect NO_x even at low or elevated temperatures makes WO_3 important for integrated sensors.[3,7]

The properties and applications of low-dimensional materials are governed mainly by the crystal structure, chemical composition, surface morphology, chemical and thermal stability, porosity, and phase stability of the resulting structures. A profound knowledge of the structure and stability of WO_3 thin films is, therefore, of importance for its effective use in practical device applications. However, inconsistent results are reported in the literature, despite the large number of studies on the structure, chromogenic effects, and electronic properties of WO_3 thin films. Thus, there is still the need to better understand the basic aspects of the phase transformations of WO_3-based materials, particularly in thin films and nanostructures, because some of their applications require annealing and/or higher temperatures for operation. From this point of view, we have investigated the structure and phase transformations in WO_3 thin films prepared by pulsed-laser deposition (PLD), which is an attractive choice for growing high-quality oxides. The excellent capability for reactive deposition in the presence of gases and the high energy of the laser-produced plasma makes PLD a promising technique for producing highly crystalline and dense films at relatively low temperatures.[12]

Different crystal phases of WO_3 have been investigated using experimental and theoretical approaches in recent years.[13−17] Electron microscopy and diffraction techniques have been employed in this work to investigate the high-temperature phases of PLD WO_3 films. This technique is well suited to studying ultramicrostructures, which often arise from atomistic and molecular-level processes of low-dimensional materials.[18] Preliminary results of this work have been reported already.[19] The emphasis in this work is to characterize the growth behavior, crystal structure, surface morphology, and chemical composition of freshly grown PLD WO_3 films and to understand the effect of annealing temperature on the phase stability. The results obtained are presented and discussed in this paper. It is expected that the results offer guidance on optimizing the conditions to enhance the performance of WO_3 films in device applications.

II. Experimental Section

A. Preparation of Targets and WO_3 Thin Films. Thin films of WO_3 were produced by the multipulse laser ablation of pure WO_3 targets. The targets were prepared from commercial WO_3 (99.9%) powder. The pressed WO_3 target was heated at a rate

* Corresponding author. E-mail: ramanacv@umich.edu. Tel: 1-734-763-5344. Fax: 1-734-763-4690.

† Nanoscience and Surface Chemistry Laboratory, Department of Geological Sciences, University of Michigan.

‡ Materials Science and Engineering, University of Michigan.

§ Université Pierre et Marie Curie.

10.1021/jp056664i CCC: $33.50
Published on Web 05/11/2006

of 10 °C/min and sintered at 950 °C for about 30 h. WO_3 film fabrication was performed by irradiating the targets, preexamined for microstructure, with a KrF excimer laser ($\lambda = 248$ nm). The laser beam was incident on the target surface at an angle of 45°, and the laser flux produced (after focusing) was 2 J·cm^{-2}. During laser ablation, the target was rotated at a rate of 10 rotations per minute to avoid depletion of the material or burning deep holes at the laser spot. In addition, preliminary pulses were applied, prior to the film deposition, to remove the last contaminants and impurities present on the uppermost layer of the target. During this process, a shutter was introduced halfway between the target and the substrate. The deposition was performed onto well-cleaned glass substrates. The substrate temperature (T_s) was 300 °C during deposition. The target-to-substrate distance was 4 cm. The chamber base pressure was 1×10^{-6} Torr prior to film deposition. For reactive deposition, pure oxygen gas was introduced (using a flow controller) into the chamber and the oxygen partial pressure (pO_2) was maintained at 100 mTorr. WO_3 films were fabricated with a thickness ranging from 200 to 500 nm.

B. Characterization. In the present study, two different sets of experiments were performed. In the first set of experiments, the WO_3 films were characterized by studying their crystal structure using X-ray diffraction (XRD) and selected area electron diffraction (SAED), surface/interface structure using transmission electron microscopy (TEM), chemical characteristics using X-ray photoelectron spectroscopy (XPS) and energy-dispersive X-ray spectroscopy (EDX), surface morphology using scanning electron microscopy (SEM) and atomic force microscopy (AFM), and local structure using Raman scattering spectroscopy (RS). These measurements were made ex situ at room temperature. The stability of the PLD WO_3 films was studied in the second set of experiments using TEM and SAED. The specimen for cross-sectional TEM was prepared by the following procedure: (i) attaching silicon substrates on the surface of WO_3 film with using M-bond 610; (ii) polishing the cross-section specimen to a thickness of a few tens of micrometers and attaching the 3-mm Cu grid with a hole size of 1×2 mm; and (iii) finally, polishing the TEM specimen by precision ion milling system (GATAN, PIPS).

XRD was performed using a Philips X'Pert PRO MRD (PW3050) diffractometer equipped with a Cu anticathode (Cu Kα radiation; $\lambda = 1.54056$ Å). XPS analysis was performed using a Kratos Axis Ultra XPS system employing a monochromatic Al Kα X-ray source ($h\nu = 1486.6$ eV). Detailed scans recorded with 10 eV pass energy and 0.1 eV step size were used for composition analysis. AFM experiments were performed using a Digital Instruments AFM (Dimension 3100 series) in both contact mode and tapping mode. SEM was performed using a JEOL (Model 6150) scanning electron microscope. Raman spectra of the samples were recorded, in the wavenumber range of 20−1100 cm^{-1}, using a Jobin-Yvon U-1000 double monochromator equipped with two holographic gratings. The light scattering was detected with an ITT-FW130 cooled photomultiplier tube coupled with a computerized photon-counting system. The excitation source was the 514.5 nm line of an Ar^+ ion laser operating at a power level of 40 mW.

TEM analysis was performed using a JEOL JEM2010F at a 200 kV acceleration voltage. The spherical aberration coefficient, C_s, is 1.0 mm. The spatial resolution of this instrument is 0.10 nm for lattice resolution and 0.25 nm for point-to-point resolution. Phase transitions were monitored using SAED during heating experiments. The composition was analyzed by EDX in the TEM utilizing EDAX Genesis software. The heating sample holder and the GATAN smart heating system were used for the stability experiments in the 30−500 °C temperature range.

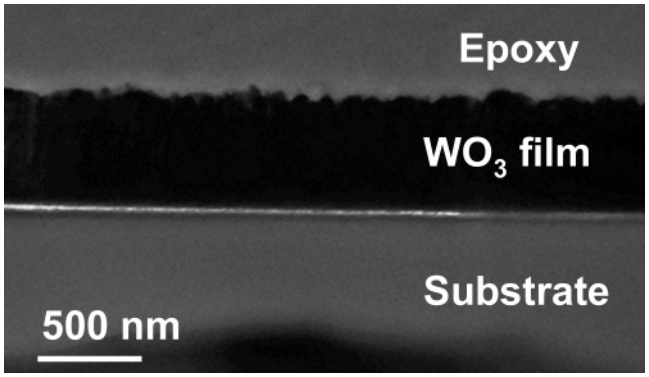

Figure 1. TEM micrograph of PLD WO_3 thin film. The bright-field view shows the sample structure containing the substrate, the WO_3 thin film, and the epoxy.

III. Results

PLD WO_3 thin films were found to be uniform and well-adherent to the substrates. The broad and diffuse XRD and Raman spectra, absence of features in SEM and AFM analysis, and complete amorphous contrast in TEM indicate that the PLD WO_3 thin films deposited at $T_s < 300$ °C were amorphous. Chemical composition analysis as a function of oxygen partial pressure in the chamber indicate that the PLD WO_3 thin films grown at $pO_2 < 100$ mTorr contain reduced species on the surface.

A. Crystal Structure and Chemical Composition. Figure 1 is a bright-field TEM image of the cross section of the sample with apparent interfaces between the substrate, the WO_3 film, and the epoxy. It is evident that the interface structure of the PLD WO_3 films is uniform. The films show some roughness (the waviness along the horizontal direction), which may be due to disorder on the surface.

The chemical analysis using XPS and EDX indicates that the freshly grown films were nearly stoichiometric without any impurities. XPS measurements (not shown) of WO_3 films grown at $T_s = 300$ °C ($pO_2 \approx 100$ mTorr) show that the atomic ratio (O/W $\approx 2.96 \pm 0.05$) is close to that of bulk WO_3. The EDX spectra shown in Figure 2 provide evidence for the chemical quality of PLD WO_3 films. The sample was positioned carefully in the TEM column to obtain the EDX spectra of the substrate (Figure 2A) and WO_3 film (Figure 2B) separately to assess the chemical quality of the films. The EDX spectrum (Figure 2B) exhibits the characteristic peaks of W and O present in the film along with that of Cu from the supporting grid. However, the absence of any other peaks except those due to W and O is evidence for the formation of W-oxide phase and chemical quality of the grown films without any elemental impurities.

The TEM results of PLD WO_3 films are shown in Figure 3. Figure 3A and B represents the high-resolution TEM (HRTEM) and the SAED images of WO_3 films, respectively. The lattice fringes observed in the HRTEM image (Figure 3A) indicate that the WO_3 film is well crystallized. The lattice fringe spacing values are 0.377 and 0.388 nm along the vertical and horizontal directions, respectively. The diffraction maxima, pertaining to the fringes observed in HRTEM image, in the corresponding SAED pattern (Figure 3B) are identified as due to reflections from the (020) and (002) lattice planes of monoclinic WO_3 (JCPDS File no. 43-1035), respectively. Thus, SAED and

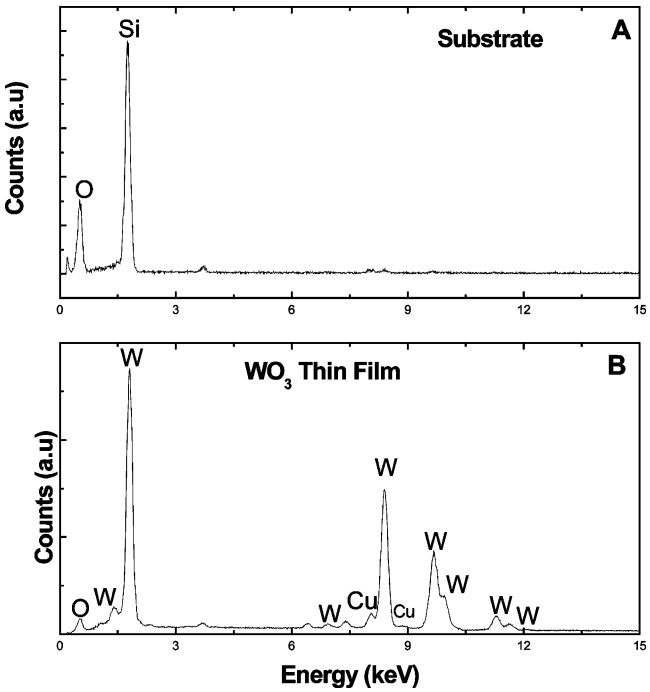

Figure 2. EDX spectra of PLD WO_3 thin films: (A) the spectrum obtained for the substrate, and (B) the spectrum obtained for the film.

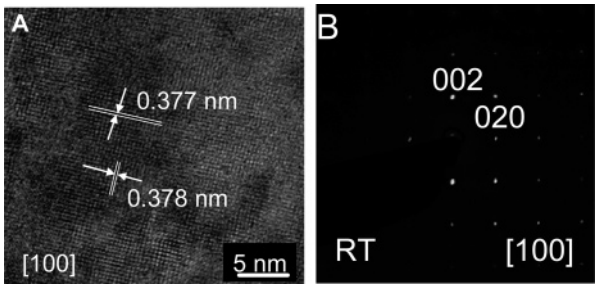

Figure 3. Electron micrographs of PLD WO_3 thin films. Image A is the HRTEM image of the PLD WO_3 thin film with lattice fringes corresponding to the monoclinic structure. Image B is the representative of the corresponding SAED pattern indicating the monoclinic WO_3.

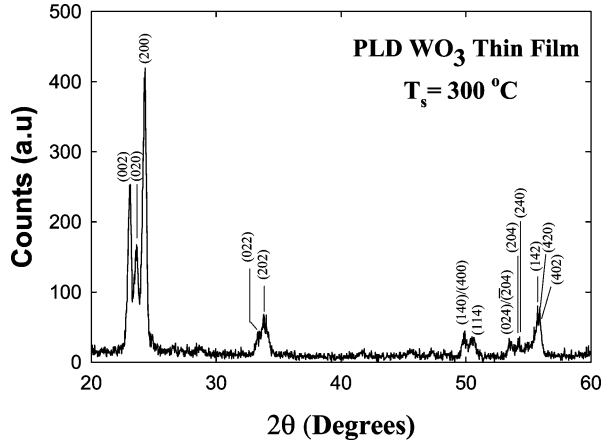

Figure 4. XRD spectrum of PLD WO_3 thin film.

HRTEM images represent the monoclinic WO_3 phase. The monoclinic phase of the freshly grown WO_3 films (T_s = 300 °C), before any annealing, was also confirmed by XRD as shown in Figure 4. The assignment of pattern was based on the monoclinic WO_3 phase (JCPDS File no. 43-1035). All of the discernible peaks in the XRD curve (Figure 4) are representative of the monoclinic phase.

B. Surface Morphology. SEM and AFM data of PLD WO_3 films are shown in Figure 5. The SEM (Figure 5A) data indicate that the films are smooth without pores, cracks, or particulates, which is important to recognize because the PLD or RPLD layers usually exhibit particulates.[12,20] AFM data indicates the existence of small grains, 50−60 nm in size, spreading uniformly on the WO_3 film surface (Figure 5B). The root-mean-square (rms) value of the surface roughness of WO_3 films evaluated from the AFM image is 10 nm. This is relatively low when compared to the 40−50 nm reported for WO_3 films grown by chemical vapor deposition methods.[21] The SEM and AFM results indicate the high surface quality of PLD WO_3 films.

C. Local Structure and Chemical Bonding. The Raman spectrum of freshly grown PLD WO_3 films is shown in Figure 6. The well-resolved peaks in the spectrum indicate that the PLD WO_3 film (T_s = 300 °C) is crystalline. Two groups of peaks can be seen in the spectrum, located in the low- and high-frequency regions. These peaks are identified as the typical Raman bands of the W−O bonds in the films: the intense peak at 520 cm^{-1}, separating the two groups of WO_3 peaks, corresponds to the zone center optical phonon of the Si substrate. The very weak peaks at 434 and 620 cm^{-1} are also related to the Si substrate. The two main peaks of the low-frequency region observed at 272 and 326 cm^{-1} can be assigned to the bending vibration $\delta(W^{6+}-O)$.[2,5,23] The peak at 303 cm^{-1} is also a deformation mode of $W^{6+}-O$ bond, which usually appears in the 270−400 region. This peak is usually seen in bulk crystals, not in films. Similarly, the intense peaks in the high-frequency region observed at 715 and 806 cm^{-1} can be assigned to the stretching vibration $\upsilon(W^{6+}-O)$.[2,5,22,23] The Raman bands observed for PLD WO_3 films are in good agreement with the those around 270 cm^{-1}, 370 cm^{-1}, 715 cm^{-1}, and 808 cm^{-1} reported for monoclinic WO_3.[2,5,23−26] The bands at 220 and 465 cm^{-1}, which are typically observed to the presence of W in the lower oxidation state,[5,22] are not observed in our samples. The RS data provide evidence for the high structural quality and supports the monoclinic phase of WO_3 films.

D. Structural Stability and Phase Transitions. The SAED patterns at different annealing temperatures obtained from exactly the same spot in the sample are shown in Figure 7. The SAED pattern shown in Figure 7A is representative of the monoclinic phase, which is stable during annealing up to ∼300 °C (Figure 7A−C). Annealing of the sample to 400 °C changes the SAED (Figure 7D). The observed diffraction maxima (Figure 7D) match only with the reflections from (001) lattice planes and (020) planes, respectively, of the orthorhombic WO_3 phase (JCPDS File no. 20-1324). Therefore, the corresponding phase is identified as orthorhombic WO_3.

The SAED pattern obtained for the sample at a temperature of 500 °C is completely different when compared to those obtained at lower annealing temperatures (Figure 7E vs Figure 7A−D). The SAED pattern clearly shows that the distance between the diffraction maxima in the vertical and horizontal directions changed significantly, indicating the transformation to the new phase. The observed diffraction pattern and the diffraction maxima were in good match with only the hexagonal phase of WO_3 (JCPDS File no. 33-1387). The diffraction maxima in the vertical and horizontal directions corresponds to the reflections from the (100) (d_{100} = 0.391 nm) and (310) (d_{310} = 0.175 nm) lattice planes, respectively, and the corresponding phase is identified as hexagonal WO_3. The SAED results indicate that the phase transitions occur from one WO_3 polymorph to the next in the sequence with increasing temperature under vacuum conditions (1.5 × 10^{-7} Torr): monoclinic

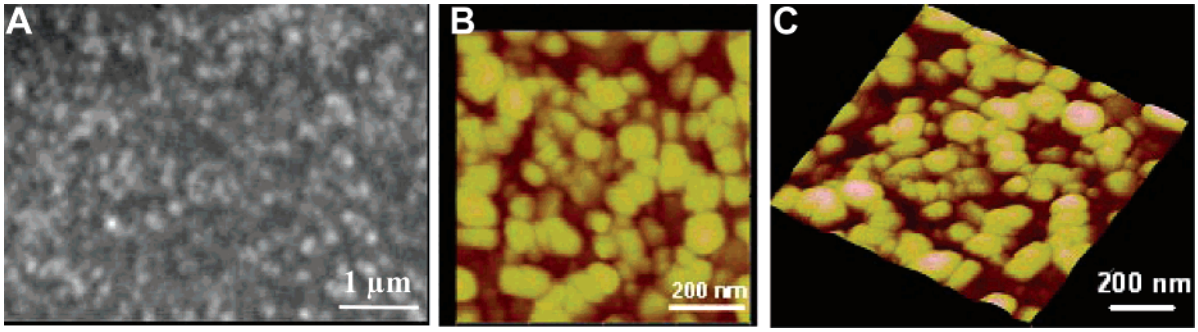

Figure 5. Surface morphology of PLD WO_3 thin films. The SEM image is shown in image A. The AFM topographic and surface three-dimensional images are shown in images B and C, respectively. The scale bar is as indicated for each of these images.

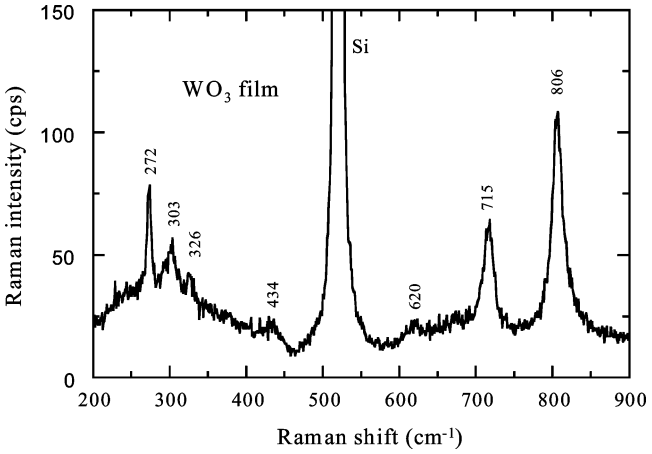

Figure 6. Raman scattering spectrum of PLD WO_3 thin film.

→ orthorhombic → hexagonal. The observed changes and the exact temperature of the phase transitions are summarized in Figure 7F.

IV. Discussion

In general, WO_3 is a complicated material with respect to crystal structure and thermal stability because of several structures, such as monoclinic, triclinic, tetragonal, orthorhombic, cubic, and hexagonal for pure and oxygen deficient WO_3.[1−3,13−17,25−29] In addition, thin films prepared by various techniques usually possess different microstructures and properties, which further change upon annealing. Therefore, it is important to characterize WO_3 films as a function of both the fabrication and the annealing conditions. Optimization of T_s and pO_2 is most important because the microstructure of WO_3 film is highly sensitive to these parameters. The XPS and EDX results indicate that the freshly grown WO_3 films are nearly stoichiometric, without any impurities, which is due mainly to the optimum pO_2 (100 mTorr). Formation of the reduced phases occurs at lower pO_2. The crystallinity of the WO_3 films is attributed to the optimum T_s (300 °C). WO_3 films grown at T_s < 300 °C were amorphous because the energy is not sufficient for the mobility of the condensed species. Structural characterization using XRD, RS, HRTEM, and SAED indicate that 300 °C is optimum to promote the crystallinity and, thus, the growth of the monoclinic WO_3.

The results of SEM and AFM provide evidence for the excellent surface quality of PLD WO_3 films in terms of low values of roughness. AFM results are also useful to understand the wavy character noticed in TEM analysis (Figure 1). The origin of the surface roughness and the observed wavy character is due to the film morphology as a result of grain structure as indicated by the AFM. Analysis using AFM, SEM, and cross-sectional TEM suggests that the growth of PLD WO_3 films does not proceed in layer-by-layer or continuous fashion but occurs by island growth. Such a growth behavior has been observed for other oxide films grown by PLD.[28,29] The important characteristic of the PLD WO_3 films is maintaining the local structure and chemical bonding as indicated by RS results. An oxygen deficiency or the defects in the films results in the reduction of W^{6+} and formation of W^{5+} and W^{4+}. The chemical bonds with W^{5+} and W^{4+} are weaker than those with W^{6+}.[5,22] Therefore, their corresponding Raman peaks appear at lower energies than those for the $W^{6+}-O$ and $W^{6+}=O$ bonds. For comparison, Stankova et al.[22] have reported the Raman bands at 220 and 465 cm^{-1} for PLD WO_3 films grown at higher temperature (600 °C) due to the presence of oxygen-deficient phases. It has been reported (based on XPS) that the defect concentration (x in WO_{3-x}) usually varies between 0.1 and 0.5 in WO_3 films.[21,23] The excellent structural quality of PLD WO_3 films, as indicated by the absence of additional Raman bands and the O/W ratio close to bulk material (XPS), is due mainly to the advantage of laser ablation process to grow stoichiometric oxides at optimum T_s and pO_2.

Despite its simple stoichiometry, the structural transformations and phase transitions of WO_3 films are quite complex. The observed phase changes in WO_3 films in the present study as a function of temperature can be explained by considering the structure of bulk WO_3. The ideal WO_3 crystal structure can be represented as a cubic ReO_3 structure.[13,30] In fact, the polymorphs of WO_3 can be described as distortions from the cubic ReO_3 structure.[1,13−16,27] The characteristic feature of the structure is that the cation is surrounded by an octahedral arrangement of oxygen atoms. Therefore, the structure is built up from a three-dimensional network of corner-sharing MO_6 (M = W or Re) octahedra as shown in Figure 8 for WO_3. The octahedral environment of W is shown in Figure 8B. The crystal structure of WO_3 can be viewed as alternating planes of O and WO_2 (Figure 8B). The planes of O and WO_2 can be viewed as placed normal to the respective crystallographic direction.

Distortions and tilting of the octahedra result in deviations from the ideal cubic ReO_3 structure, giving rise to a series of lower symmetry structures.[13−17,26,27] Predominant distortion mechanisms responsible for phase transformations include tilting of the WO_6 octahedra, displacements of the W atoms from the center of the octhedra, and distortions of the octahedra. In the monoclinic WO_3 phase, the unit cell contains eight WO_6 octahedra and the average distance between neighboring W atoms is 0.375 nm. PLD WO_3 films grown at 300 °C exhibit the monoclinic phase, which is found to be stable during sample heating to a temperature of ∼350 °C, at which point there is direct transition to the orthorhombic phase. However, the possibility of a transition from monoclinic to triclinic or

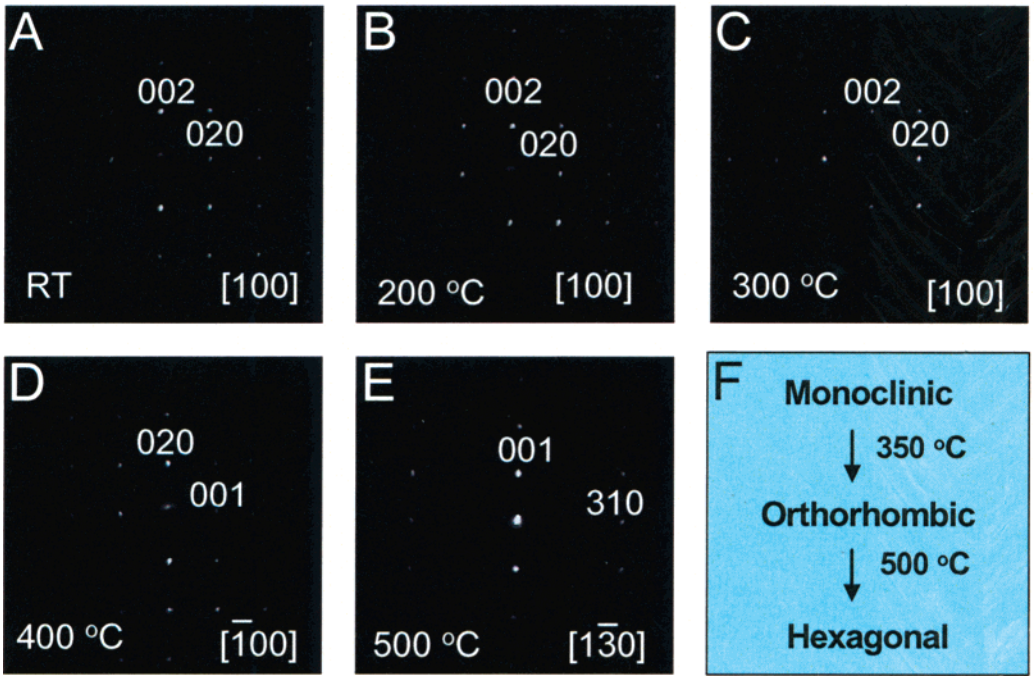

Figure 7. Electron diffraction patterns of PLD WO_3 thin films as a function of annealing temperature. Images A, B, and C represent the patterns obtained for PLD WO_3 thin films at temperatures RT, 200 °C, and 300 °C, respectively, indicating the stability of the films in monoclinic structure up to the transition to the orthorhombic phase at 350 °C. Images D and E represent the electron diffraction patterns obtained at temperatures 400 °C and 500 °C, respectively. The indices for the observed spots are indicated in the images. Image F summarizes the structural changes and transition temperatures.

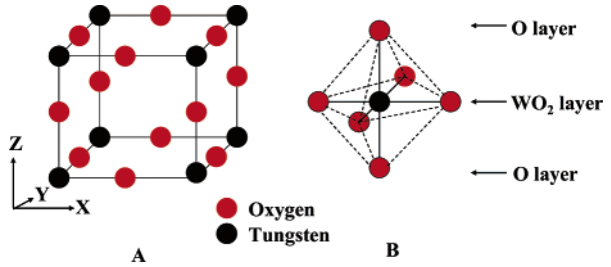

Figure 8. The structure of WO_3. (A) The ideal cubic structure of WO_3. (B) The WO_6 octahedra. The visualization of alternating WO_2 and O planes is also indicated.

coexistence of monoclinic and triclinic phases before the transition to orthorhombic phase cannot be eliminated because it is hard to distinguish between these two as they are structurally similar. The transition temperature (350 °C) at which the orthorhombic phase appears for PLD WO_3 films is close to 320 °C reported for bulk WO_3.[29] The phase boundary from the monoclinic to the orthorhombic phase is characterized by a decrease in the W−O displacement along the (001) direction, which is possible by shifting W atoms and by tilting the WO_6 octahedra. In a similar way, orthorhombic WO_3 transforms to a hexagonal WO_3 phase. However, the orthorhombic to hexagonal phase is not usual in bulk WO_3. Previous investigations on bulk WO_3 report the following sequence: triclinic (~30 °C) → monoclinic (330 °C) → orthorhombic (740 °C) → tetragonal.[14,16] In fact, the hexagonal phase of WO_3 is a new phase identified only in the early 1980s.[31] However, Mohammad and Gillet have recently observed the hexagonal phase in thermally evaporated (TE) WO_3 films using TEM, and the origin was attributed to the initial hydration and subsequent dehydration during annealing at >200 °C and similarity of the $WO_3 \cdot (^1/_3)H_2O$ and hexagonal WO_3 phases. Another remarkable difference is that the transformation to orthorhombic phase, as observed in PLD WO_3 films, was not observed in TE WO_3 films. The authors explained that the orthorhombic structure formed during annealing above 330 °C may reversibly be transformed to monoclinic phase by the time of TEM observation, which was performed when the temperature was decreased to room temperature. The origin of the hexagonal phase in PLD WO_3 films is not clear. To conclude, the information presented, herein in this paper, on the structure of freshly grown materials and structural stability and phase transformations as a function of temperature could be useful while considering the PLD WO_3 thin films for technological applications.

Acknowledgment. The authors at the University of Michigan acknowledge the support of the National Science Foundation (NSF-NIRT, EAR-0403732).

References and Notes

(1) Granqvist, C. G. *Handbook of Inorganic Electrochromic Materials*; Elsevier: New York, 1995.

(2) Santato, C.; Odziemkowski, M.; Ulmann, M.; Augustynski, J. *J. Am. Chem. Soc.* **2001**, *123*, 10639.

(3) Djerad, S.; Tifouti, L.; Crocoll, M.; Weisweiler, W. *J. Mol. Catal. A Chem.* **2004**, *208*, 257.

(4) Huguenin, F.; Gonzalez, E. R.; Oliveira, O. N., Jr. *J. Phys. Chem. B* **2005**, *109*, 12837.

(5) Lee, S.-H.; Choeng, H. M.; Zhang, J.-G.; Mascarenhas, A.; Benson, D. K.; Deb, S. K. *Appl. Phys. Lett.* **1999**, *74*, 242.

(6) Trasferetti, C. B.; Rouxinol, F. P.; Gelamo, R. V.; Bica de Moraes, M. A.; Davanzo, C. U.; de Faria, D. L. A. *J. Phys. Chem. B* **2004**, *108*, 12333.

(7) Satnkova, M.; Vilanova, X.; Llobet, E.; Calderer, J.; Bittencourt, C.; Pireaux, J. J.; Correig, X. *Sens. Actuators, B* **2005**, *105*, 271.

(8) Gavrilyuk, A. I. *Electrochim. Acta* **1999**, *44*, 3027.

(9) Li, M.; Gao, W.; Posadas, A.; Ahn, C. H.; Altman, E. I. *J. Phys. Chem. B* **2004**, *108*, 15259.

(10) Soto, G.; Cruz, W. D. L.; Diaz, J. A.; Castillon, F. F.; Farias, M. H. *Appl. Surf. Sci.* **2003**, *218*, 281.

(11) Ma, S.; Frederick, B. G. *J. Phys. Chem. B* **2003**, *107*, 11960.

(12) *Pulsed Laser Deposition of Thin Films*; Chrisey, D. G., Hubler, H. K., Eds.; Wiley Publications: New York, 1994.

(13) Cora, F.; Stachiotti, M. G.; Catlow, C. R. A.; Rodriguez, C. O. *J. Phys. Chem.* **1997**, *101*, 3945.
(14) Vogt, T.; Woodward, P. M.; Hunter, P. A. *J. Solid State Chem.* **1999**, *144*, 209.
(15) Chatten, R.; Chadwick, A. V.; Rougier, A.; Lindan, P. J. D. *J. Phys. Chem. B* **2005**, *109*, 3146.
(16) Cazzanelli, E.; Vinegoni, C.; Mariotto, G.; Kuzmin, A.; Purans, J. *J. Solid State Chem.* **1999**, *143*, 24.
(17) Perez, M. A.; Lopez Teijelo, M. *J. Phys. Chem. B* **2005**, *109*, 19369.
(18) Utsunomiya, S.; Ewing, R. C. *Environ. Sci. Technol.* **2003**, *37*, 786.
(19) Ramana, C. V.; Utsunomiya, S.; Ewing, R. C.; Julien, C. M.; Becker, U. *Phys. Status Solidi A* **2005**, *202*, R108.
(20) Bauerle, D. *Laser Processing and Chemistry*; Spinger: Berlin, 1996.
(21) Tanner, R. E.; Szekeres, A.; Gogova, D.; Gesheva, K. *Appl. Surf. Sci.* **2003**, *218*, 162.
(22) Stankova, N. E.; Atanasov, P. A.; Stanimirova, T. J.; Dikovska, A. Og.; Eason, R. W. *Appl. Surf. Sci.* **2005**, *247*, 401.
(23) Rougier, A.; Portemer, F.; Quede, A.; Marssi, M. El. *Appl. Surf. Sci.* **1999**, *153*, 1.
(24) Bittencourt, C.; Landers, R.; Llobet, E.; Correig, X.; Calderer, J. *Semicond. Sci. Technol.* **2002**, *17*, 522.
(25) Haro-Poniatowski, E.; Jounnae, M.; Morhange, J. F.; Julien, C.; Diamant, R.; Fernandez-Guasti, M.; Fuentes, G. A.; Alonso, J. C. *Appl. Surf. Sci.* **1998**, *127*, 674.
(26) Salje, E. K. H.; Rehmann, S.; Pobell, F.; Morris, D.; Knight, K. S.; Herrmannsdorfer, T.; Dove, M. T. *J. Phys.: Condens. Matter* **1997**, *9*, 6563.
(27) Patil, P. S. *Bull. Mater. Sci.* **2000**, *23*, 309.
(28) Ramana, C. V.; Smith, R. J.; Hussain, O. M.; Julien, C. M. *J. Vac. Sci. Technol., A* **2004**, *22*, 2453.
(29) Ramana, C. V.; Smith, R. J.; Hussain, O. M.; Chusuei, C. C.; Julien, C. M. *Chem. Mater.* **2005**, *17*, 1213.
(30) Rao, C. N. R.; Raveau B. *Transition Metal Oxides*; VCH: New York, 1995.
(31) Gerand, B.; Nowogrocki, G.; Guenot, J.; Figlarz, M. J. *J. Solid State Chem.* **1979**, *29*, 429.
(32) Al Mohammad, A.; Gollet, G. *Thin Solid Films* **2002**, *408*, 302.